

Spin-charge separation in cold Fermi-gases: a real time analysis

C. Kollath,¹ U. Schollwöck,¹ and W. Zwerger²

¹*Institute for Theoretical Physics C, RWTH Aachen, D-52056 Aachen, Germany*

²*Physics Department, Technical University Munich, D-85748 Garching, Germany*

(Dated: August 18, 2018)

Using the adaptive time-dependent density-matrix renormalization group method for the 1D Hubbard model, the splitting of local perturbations into separate wave packets carrying charge and spin is observed in real-time. We show the robustness of this separation beyond the low-energy Luttinger liquid theory by studying the time-evolution of single particle excitations and density wave packets. A striking signature of spin-charge separation is found in 1D cold Fermi gases in a harmonic trap at the boundary between liquid and Mott-insulating phases. We give quantitative estimates for an experimental observation of spin-charge separation in an array of atomic wires.

One-dimensional (1D) quantum many-body systems have been at the center of theoretical and experimental interest for the last two decades. Following the seminal work of Haldane [1], it has been understood that - independent of their bosonic or fermionic nature - the low-energy behaviour of 1D quantum liquids is universally described by the so-called Luttinger liquid (LL) picture [2, 3]. Probably the most remarkable prediction is the phenomenon of spin-charge separation in the case of Fermions, i.e. the fact that - at low energy - the excitations of charge and spin completely decouple and propagate with different velocities. A definite signature of spin-charge separation requires the observation of the two corresponding branches of excitations in the single particle spectral function [18]. In condensed matter systems, numerous experiments have looked for spin-charge separation e.g. via photoemission from 1D metallic wires on surfaces [4], in 1D organic wires [5], in carbon-nanotubes [6], and in quantum wires in semiconductors, where the singular nature of the spectral functions associated with spin-charge-separation was observed in tunneling experiments [7]. In the last few years, ultracold gases in optical lattices are providing an entirely new area of physics where strong correlations can be studied with unprecedented control and tunability of the parameters. In particular these systems open the possibility to investigate the transition between three, quasi-two and quasi-one dimension. Recently, an 'atomic quantum wire' configuration in an array of thousands of parallel atom waveguides was realized in ultracold Fermi gases by the application of a strong two dimensional optical lattice [8]. The possibility to use cold atoms for studying the phenomenon of spin-charge separation was first suggested by Recati et al. [9]. Their analysis is essentially based on the hydrodynamic Hamiltonian of the LL; the inhomogeneity due to the presence of a harmonic trap is treated within a local density approximation (see also [10]). In practice, with typically less than 100 atoms per atomic wire [8], observable effects require to use stronger and more localized perturbations, where a LL description is not applicable. In addition, the effect of boundaries, where the local density approximation breaks down, are of cru-

cial importance. For a quantitative description of spin-charge separation in 1D cold Fermi gases, it is thus necessary to use a microscopic description like the Hubbard model and properly treat the inhomogeneous case with realistic system sizes. Due to the short range nature of the interactions between cold atoms, the Hubbard model is indeed a perfect description of a situation, in which there is an additional optical lattice along the weakly confined axial direction (for bosons, the corresponding setup has already been realized, see [11, 12]). It is an essential new feature of cold atoms in optical lattices that parameters can be changed dynamically and the resulting time evolution can be studied. This gives direct access to the real-time dynamics of strongly correlated systems, a subject hardly studied so far. In this context, a successful method is the recently developed adaptive time-dependent density matrix renormalization group (adaptive t-DMRG) [13] which is an efficient implementation of Vidal's TEBD algorithm [14] in the DMRG framework [15]. It has previously been applied to study density perturbations in bosonic 1D condensates over a large range of interaction strengths [16]. The real-time dynamics of interacting spinful Fermionic systems is much harder and has not been studied except for very small systems [17]. In our present work, we present numerical results of the real-time dynamics of a 1D Hubbard model for realistic sizes of up to 128 sites. Our main results are:

- (i) real-time calculation showing spin-charge separation explicitly in systems of experimentally accessible size
- (ii) the demonstration that spin-charge separation survives far outside the low-energy LL regime
- (iii) a quantitative calculation for the effect of spin-charge separation at the boundary between a liquid and a Mott-insulating (MI) phase which allows to observe the phenomenon in cold gases without the problems arising from the different densities in an array of parallel atomic wires and to distinguish experimentally between a Mott- and a band insulator.

Our starting point is the standard Hubbard model

$$H = -J \sum_{j,\sigma} (c_{j+1,\sigma}^\dagger c_{j,\sigma} + h.c.) + U \sum_j n_{j,\uparrow} n_{j,\downarrow}$$

$$+ \sum_{j,\sigma} \varepsilon_{j,\sigma} \hat{n}_{j,\sigma} \quad (1)$$

for Fermions in 1D. Its parameters are the hopping matrix element J , the on-site repulsion $U > 0$ between Fermions of opposite spin $\sigma = \uparrow, \downarrow$ at sites $j = 1, \dots, L$ and a spin-dependent local on-site energy $\varepsilon_{j,\sigma}$, describing both a possible smooth harmonic confinement and time-dependent local potentials. One introduces a 'charge' density $n_c = n_\uparrow + n_\downarrow$ and a 'spin' density $n_s = n_\uparrow - n_\downarrow$; in a realization with cold gases, the spin degrees of freedom are represented by two different hyperfine levels, and 'charge' density is particle density. Similar to bosons in an optical lattice [19], the ratio $u = U/J$ can easily be changed experimentally by varying the depth V_0 of the optical lattice. We use units where both J and \hbar are equal to one; thus time is measured in units of \hbar/J . In the numerical calculations below, we study the dynamics of the Hubbard model using different initial density perturbations and the excitations resulting from adding a single particle at a given lattice site, which is expected to display the same physics as contained in single particle spectral functions. Experimentally, the density perturbations may be generated by a blue- or red-detuned laser beam tightly focused perpendicular to an array of atomic wires, which generates locally repulsive or attractive potentials for the atoms in the wires. In practice, the perturbations due to an external laser field are quite strong, typically of the order of the recoil energy E_r and thus clearly require a non-perturbative treatment. In our calculations the length of the chains was chosen up to $L = 128$ sites, keeping of the order of several hundred DMRG states. DMRG error analysis reveals that all density distributions shown here are exact for all practical purposes, with controlled errors of less than $O(10^{-3})$ [20].

We start with a homogeneous system which is perturbed by a potential $\varepsilon_{j,\uparrow}$ localized at the chain center which couples only to the \uparrow -Fermions, i.e.

$$\varepsilon_{j,\uparrow}(t) \propto \exp \{-[j - (L-1)/2]^2/8\} \theta(-t) \quad (2)$$

The potential is assumed to have been switched on slowly enough for equilibration, and is then switched off suddenly at time $t = 0$. In Fig. 1 (a) the density distribution of the state at $t = 0.2$ is shown. The external potential (2) generates a dominant perturbation in the \uparrow -Fermion distribution by direct coupling and, indirectly, a smaller perturbation in the \downarrow -density due to the repulsive interaction between the different spin species. The wave packets in \uparrow and \downarrow -density hence perform a complicated time evolution (Fig. 1). In contrast, the perturbations in the spin and charge density split into two wave packets each moving outwards. Their respective velocities are different as indicated by the arrows in Fig. 1 (b), separating spin and charge.

In the limit of an infinitesimal perturbation much broader than the average interparticle spacing, both spin

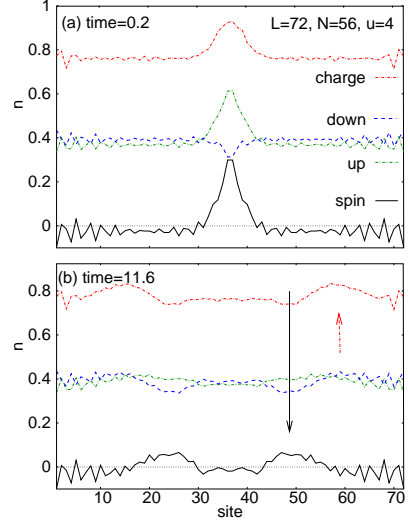


FIG. 1: Snapshots of the evolution of the density distribution are shown at different times. At $t = 0.2$, a wave packet is present in the center of the system in both the spin and the charge density. Each of these splits up into two packets which move with the same velocity in opposite directions. The velocity of the charge wave and the spin wave are different.

and charge velocities are known analytically from the Bethe ansatz [21]. To compare our numerical findings to the exact charge velocity, we create pure charge density perturbations, by applying the potential of Eq. (2) to both species, i.e. $\varepsilon_{j,\uparrow} = \varepsilon_{j,\downarrow}$, and calculate their time-evolution after switching off the potential. The charge velocity is determined from the propagation of the maximum (minimum) of the charge density perturbation for bright ($\eta_c > 0$) and grey ($\eta_c < 0$) perturbations, respectively. In Fig. 2 the charge velocities for various background densities n_0 and perturbation amplitudes η_c are shown. We find good agreement, if we plot the charge velocity versus the charge density at the maximum (minimum), i.e. $n_c = n_0 + \eta_c$. This stays true even for strong perturbations $\eta_c \approx \pm 0.1$ which corresponds to 20% of the charge density. The charge velocity is thus robust against separate changes of the background density n_0 and the height of the perturbation η_c . By contrast, the velocity of a spin perturbation varies strongly with its height. A possible reason for this may be the nonlinear $\cos \phi$ -contribution in the LL description of the spin density field, which is only marginally irrelevant, giving rise to a nonanalytic contribution to the spin-density response [3]. Nevertheless, our numerical results show that for decreasing height of the spin perturbation, its velocity approaches the value for the spin velocity obtained by the Bethe ansatz.

In order to compare the behaviour of the density perturbations with that of a single particle excitation, the time evolution of the system with one additional particle

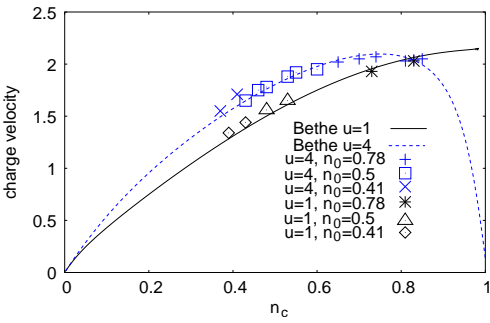


FIG. 2: Exact results for the charge velocity obtained by the Bethe ansatz are (lines) compared to the numerical results of the adaptive t-DMRG. The numerical results correspond to different heights of the perturbations at various charge background densities n_0 . n_c is the charge density at the maximum/minimum of the charge density perturbation. The uncertainties are of the order of the size of the symbols and stem mainly from the determination of the velocity.

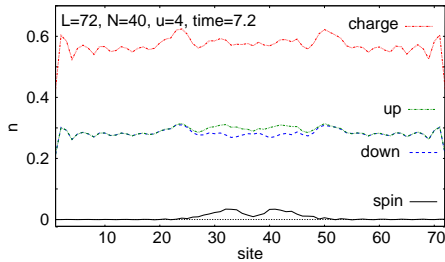


FIG. 3: Snapshot of the time-evolution of the charge and spin densities of a single particle excitation created at time $t = 0$ at site $j = 37$ is shown for $t = 7.2$.

added at time $t = 0$ on site j to the ground state, is calculated numerically. In Fig. 3 a snapshot of the resulting evolution of the densities is shown for time $t = 7.2$. Remarkably, as in the case of the density perturbation separate wave packets in spin and charge can be seen. This demonstrates the phenomenon of spin-charge separation directly in a single particle excitation, in close analogy to the situation of an inverse photo-emission experiment for the single particle spectral functions [4].

In a specific experiment with arrays of parallel atomic wires, it is necessary to take into account that there is an additional harmonic trapping potential. Moreover, individual wires have slightly different fillings, which leads to an inhomogeneous broadening due to the resulting difference in velocities. In order to observe an unambiguous signal of spin-charge separation in such a situation, we suggest an experimental setup, which relies on the co-existence of a MI state and a liquid state in spatially separated regions of the parabolically confined system [22]. The idea is to use the very different behaviour of the charge and spin degrees of freedom in the MI phase.

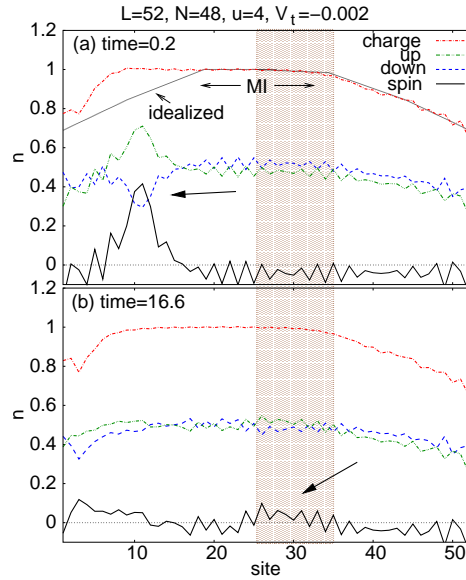


FIG. 4: Time-evolution of charge and spin density perturbations in the presence of a parabolic trapping potential $\varepsilon_{\sigma,j} = -V_t a^2 (j - L/2 + 0.5)^2 E_r$. MI marks the approximate MI region in the absence of the perturbation. The line denoted by idealized is a sketch of the charge density distribution without the perturbation. The presence of the perturbation enlarges the region in which the charge density is locked to $n_c = 1$. The arrows show the approximate place of the spin perturbation, and the shaded region marks the region over which the densities are averaged (cf. Fig. 5).

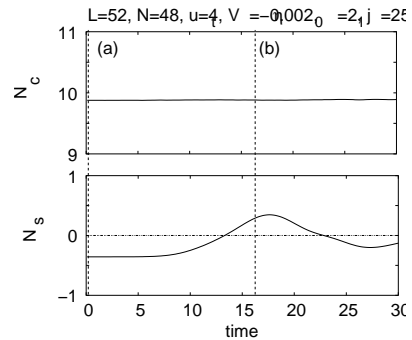


FIG. 5: Time evolution of the charge and spin density summed over the sites $j_0 = 25$ to $j_1 = 35$. Vertical lines correspond to the times of the snapshots in Fig. 4

In this phase the charge excitation spectrum has a gap, whereas the spin dispersion is still linear for small momenta, and the spin velocity is finite. By contrast, in the liquid phase both excitation spectra are linear for small momenta. To exploit this, assume the system of one-dimensional wires is prepared in such a way, that a MI region is present in the center, where the charge density is locked at half-filling, $n_c = 1$. At the boundary of this MI region liquid regions appear. A localized potential in

the liquid region will then create spin and charge density waves. Calculated snapshots of the time evolution in such a situation are shown in Fig. 4. Evidently, the spin density wave propagates into the MI region whereas the charge density perturbation is almost completely reflected due to the charge gap in the MI. The presence of spin density oscillations which are due to the antiferromagnetic coupling induced by the interaction obscures the exact evolution of the spin perturbation. However by averaging over several lattice sites - as is always necessary in an experiment - the effect of spin-charge separation is clearly visible. In Fig. 5 examples for the evolution of the sum of the charge and the spin number of particles between site 25 and 35, N_c and N_s respectively, are shown. It is clearly seen that the sum of the charge occupation does not change, whereas the spin occupation shows the moving wave packet. The average spin velocity can be determined from Fig. 5 if the distance between the localized potential which generates the perturbation and the center of the region over which the density is measured is known. Here, the spin velocity is found to be $v_s \approx 1.1J/\hbar$ which agrees nicely within the expected accuracy with the value of $v_s(n_c = 1) = 1.2J/\hbar$ of the Bethe ansatz. The very different propagation behaviour of charge and spin can as well be used experimentally to distinguish between a MI and a band insulator: In a band insulator not only the velocity of the charge, but as well of the spin would vanish, whereas, as used above, in the MI the spin velocity stays finite.

In order to quantify the requirements for an experimental observation of spin-charge separation in cold Fermi gases, we finally discuss typical parameters which need to be achieved in a setup with an array of atomic wires [8]. Such an array consists of several thousand parallel wires with typically less than 100 ^{40}K atoms each. In addition to the smooth axial confinement potential with frequency $\omega_z \approx \varepsilon_F/N \approx 2\pi \cdot 275\text{Hz}$ (corresponding to $V_t \approx -0.0035$), realization of a 1D Hubbard model requires adding a strong periodic potential along the tubes. For ^{40}K and a standard lattice constant $a = 413\text{nm}$ the recoil energy is $E_r \approx 7\text{kHz}$. An optical lattice of height $V_0 = 15E_r$ then gives an on-site repulsion $U \approx 0.17E_r$, where we have used a standard value for the s-wave scattering length $a_s \sim 174a_0$ for the $F = 9/2$ $m_f = -9/2$ and $m_f = -7/2$ states [23]. The resulting dimensionless interaction $u \approx 22$ then leads to a central MI region with a typical size of around 20 sites. With this parameters, the time in which the spin wave travels 20 sites is of the order of a few ms. The creation of state selective potentials for two different hyperfine states may be done by using laser light whose frequency falls between the respective transitions. This might be difficult for the $F = 9/2$ $m_f = -9/2$ and $m_f = -7/2$ levels, but should be possible - for instance- using the $F = 9/2$ and $F = 7/2$ levels. The $1/e^2$ -radius of the potential (Eq. 2) is taken to be four lattice sites, which could be realized

approximately by a laser of an $1/e^2$ -radius of $2.1\mu\text{m}$ or less. Finally, to ensure that finite temperature does not destroy the Mott insulating behaviour by thermal activation, the energy scale $k_B T$ should be smaller than the Mott energy gap. Already the very first experiment of 1D fermions in an optical lattice is very close to matching those conditions. Improvements can be reached reducing the axial confinement frequency.

To conclude we have performed numerical simulations of the time-evolution of charge and spin density perturbations in the 1D Hubbard model. We clearly observe the separation of spin and charge as a generic feature of 1D fermions, far beyond the low-energy regime where a Luttinger liquid description applies. In addition, an experiment is suggested which exhibits the separation of the two modes from the perfect reflection of density excitations at the boundary to a Mott insulating state

We gratefully acknowledge very fruitful discussions with Th. Giamarchi and with the experimental group of T. Esslinger, in particular H. Moritz.

- [1] F. D. M. Haldane, J. Phys. C: Solid State Phys. **14**, 2585 (1981); Phys. Rev. Lett. **47**, 1840 (1981).
- [2] J. Voit, Rep. Prog. Phys. **58**, 977 (1995).
- [3] T. Giamarchi, *Quantum physics in one dimension*, Oxford, 2004 (Oxford University press).
- [4] P. Segovia *et al.*, Nature **402**, 504 (1999) claimed an interpretation of their photoemission data in terms of spin-charge separation. For a different view see Losio *et al.*, Phys. Rev. Lett. **86**, 4632 (2001).
- [5] T. Lorenz *et al.*, Nature **418**, 614 (2002).
- [6] M. Bockrath *et al.*, Nature **397**, 598 (1999).
- [7] O. M. Auslaender *et al.*, Science **308**, 88 (2005).
- [8] H. Moritz *et al.*, Phys. Rev. Lett. **94**, 210401 (2005).
- [9] A. Recati *et al.*, Phys. Rev. Lett. **90**, 020401 (2003).
- [10] L. Kecke, H. Grabert, W. Häusler, Phys. Rev. Lett. **94**, 176802 (2005).
- [11] T. Stöferle *et al.*, Phys. Rev. Lett. **92**, 130403 (2004).
- [12] B. Paredes *et al.*, Nature **429**, 277 (2004).
- [13] A.J. Daley *et al.*, J. Stat. Mech. (2004) P04005; S. R. White, A. Feiguin, Phys. Rev. Lett. **93**, 076401 (2004)
- [14] G. Vidal, Phys. Rev. Lett. **93**, 040502 (2004).
- [15] S. R. White, Phys. Rev. Lett. **69**, 2863 (1992). U. Schollwöck, Rev. Mod. Phys. **77**, 259 (2005).
- [16] C. Kollath *et al.*, Phys. Rev. A **71**, 053606 (2005).
- [17] Previous studies based on exact diagonalization took 3 particles in a lattice with 16 sites in E. A. Jagla, K. Hallberg, C. A. Balseiro, Phys. Rev. B **47**, 5849 (1993).
- [18] M. G. Zacher *et al.*, Phys. Rev. B **57**, 6370 (1998)
- [19] D. Jaksch *et al.*, Phys. Rev. Lett. **81**, 3108 (1998).
- [20] For a detailed error analysis see D. Gobert *et al.*, Phys. Rev. E **71**, 036102 (2005).
- [21] E.H. Lieb and F.Y. Wu, Phys. Rev. Lett. **20**, 1445 (1968). H. Shiba, Phys. Rev. B **6**, 930 (1972). C. F. Coll, Phys. Rev. B **9**, 2150 (1974). H.J. Schulz, Phys. Rev. Lett. **64**, 2831 (1990).
- [22] M. Rigol and A. Muramatsu, cond-mat/0412543 (2004).
- [23] C.A. Regal and D.S. Jin, Phys. Rev. Lett. **90**, 230404

(2003).